Active Vibration Suppression via LQG/LTR; Analytic and Experimental Results for the PACOSS Dynamic Test Article

Russell N. Gehling ‡
Martin Marietta Astronautics Group

ABSTRACT

Future large space systems (LSS) will possess high modal density at low frequencies, and mission performance requirements will necessitate control bandwidths encompassing these modal frequencies. This situation has potential for adverse controls/structure interaction (CSI) detrimental to system performance.

The Passive and Active Control of Space Structures (PACOSS) program has investigated the design, analysis, and verification of passive and active damping strategies applied to LSS. This paper discusses the results of an experiment in which a Linear Quadratic Gaussian with Loop Transfer Recovery (LQG/LTR) design technique was applied to the PACOSS Dynamic Test Article (DTA) for the purpose of high authority vibration suppression.

In general, the LQG/LTR control demonstrated high sensitivity to design model accuracy. Actual performance was significantly less than predicted, even though the control design utilized an accurate test-verified model.

The results of this experiment indicate that analytic LSS models which are quite accurate by structural dynamics standards may be insufficient for use as design models in modern control algorithms. However, passive damping designed into LSS flexible modes will simplify the active control design and implementation in terms of sensor/actuator requirements, design model order, real time computing requirements, and overall system robustness.

‡ P.O. Box 179, Denver, CO. 80201, Mail Stop H4330, phone: (303) 971-9388.

INTRODUCTION

Future large space systems (LSS) will possess high modal density at low frequencies. Some missions envisioned for these systems require rapid retargeting and precision pointing which lead to control bandwidths overlapping many closely spaced structural modes. Therefore, some means of structural vibration control will be necessary to avoid excessive excitation of the flexible modes. Passive/active vibration control is the most realistic and efficient approach for vibration suppression in such dynamically challenging systems

The Passive and Active Control of Space Structures (PACOSS) program investigated the design and implementation of passive and active vibration suppression on structures typical of many LSS configurations. This involved design and fabrication of the passively damped dynamic test article (DTA) possessing high modal density between 1 and 10 Hz (Fig 1). Also, an active vibration control system was designed and implemented. A brief description of the DTA hardware and test setup is presented in this paper, while a detailed description of the DTA is given in Reference 1.

Previous investigations with the DTA demonstrated good agreement between measured and predicted performance of the passive damping design acting in concert with local direct velocity feedback (LDVFB) as discussed in Reference 2. However, the LDVFB was a relatively low authority active damping approach which did not dramatically improve the DTA line of sight (LOS) performance. Optimal control in the form of a Linear Quadratic Regulator (LQR) approach allows for efficient use of actuator capability in the design of high authority vibration control. The loop transfer recovery (LTR) technique allows for estimator design which recovers the desirable characteristics of the LQR full state feedback design. These characteristics make the LQG/LTR design algorithm attractive for designing a multi-input multi-output vibration controller for the DTA.

This paper discusses the application of the LQG/LTR control design algorithm to the DTA LOS vibration suppression problem. Analytic and measured results are presented to show the degree of agreement between analytic predictions and actual performance. Conclusions regarding the practical application of LQG control for vibration suppression and the role of passive damping are drawn from the test results and analytic studies.

HARDWARE DESCRIPTION AND MODELING

The PACOSS DTA is a laboratory testbed for passive and active structural vibration control implementation and testing. The DTA possesses 23 major structural modes between 1 and 10 Hz, many of which are global in nature. Using the methods described in Reference 3, passive damping levels between 5% and 10% (modal viscous) were designed into the flexible modes which contribute to LOS error. The analytic model was then verified through a comprehensive modal survey (Reference 4). The DTA is suspended from three pneumatic suspension devices which have very low stiffness and virtually no friction. The suspension arrangement gives the DTA six rigid body modes below 0.3 Hz. The overall test setup is shown in Figure 2.

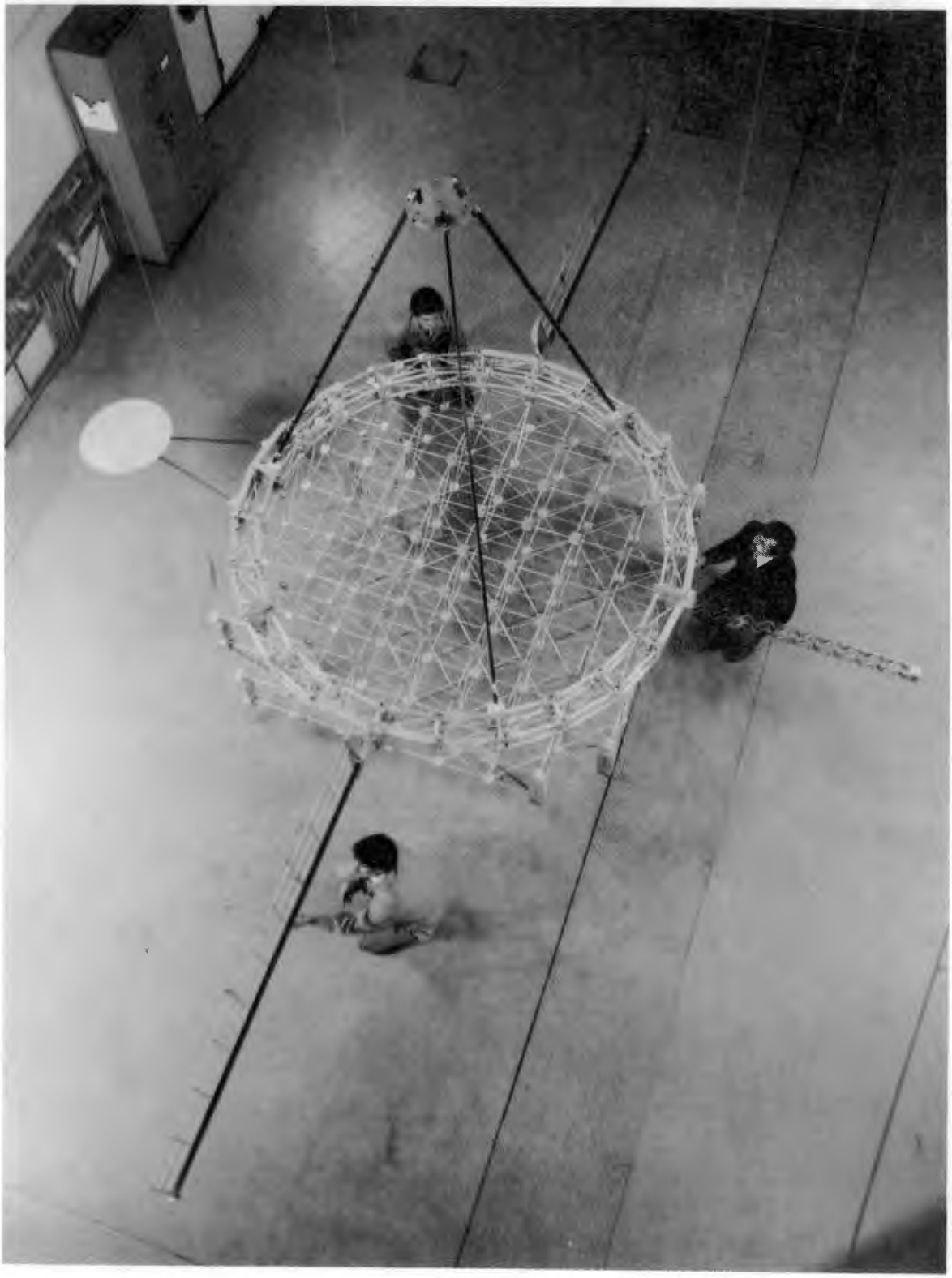

Figure 1 PACOSS Dynamic Test Article

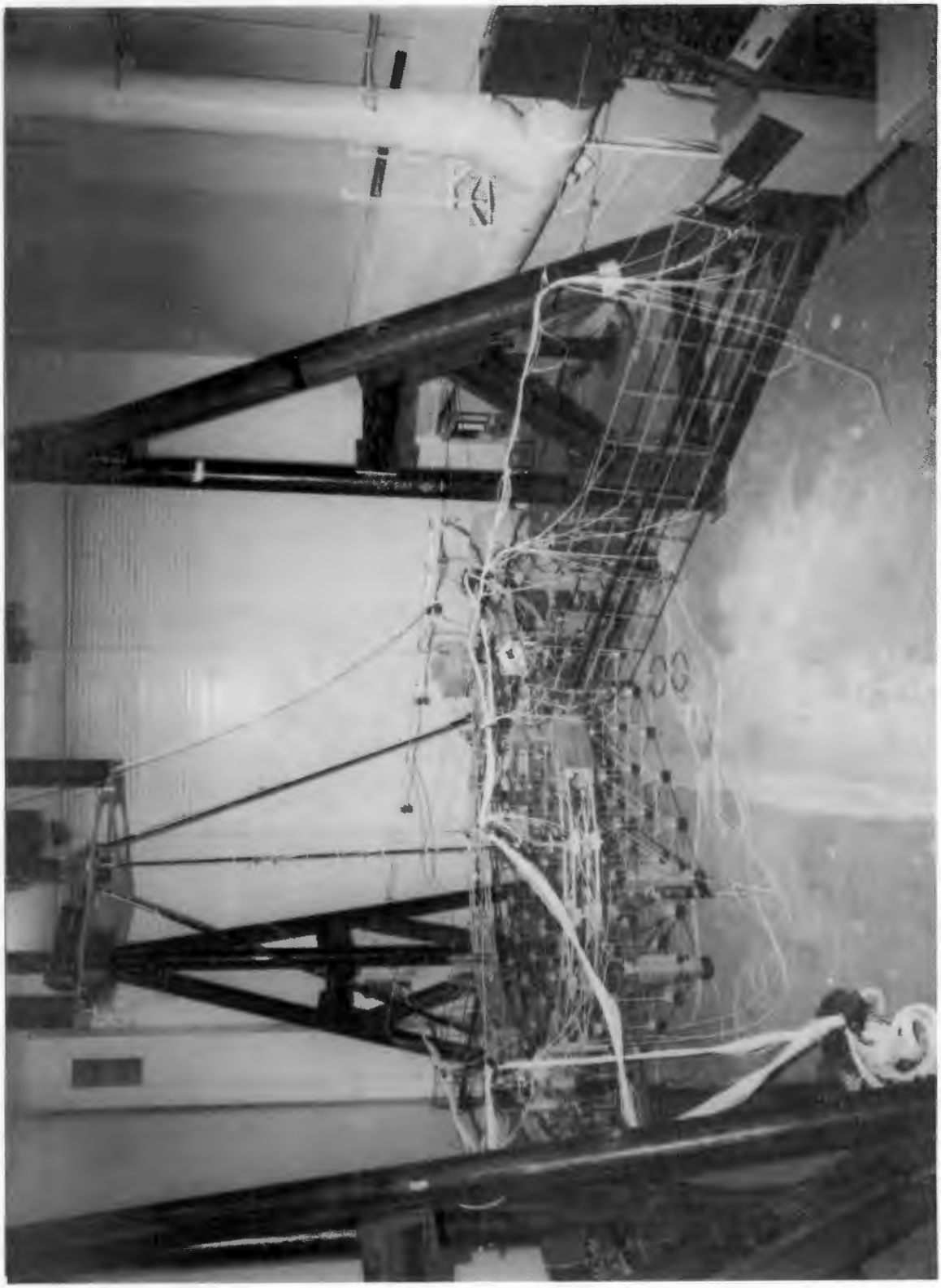

Figure 2 DTA Test Setup

The active control system includes reaction mass actuators (RMA), inertial velocity measurements, and a digital control processor. Ten RMAs with collocated Sundstrand QA-1400 accelerometers and linear velocity transducers are mounted at the locations shown in Figure 3. Also identified in Figure 3 are the locations of three additional non-collocated QA-1400 accelerometers. Inertial velocity is obtained from the 13 accelerometers by integrating the signals with bi-quad filters as discussed in Reference 5. Thus, the control system involves 23 inputs (10 collocated inertial velocities, 10 collocated relative velocities between the reaction masses and DTA, and 3 non-collocated inertial velocities),and 10 outputs. Control laws are implemented via an Optima/3 digital controller capable of handling up to 32 inputs and 32 outputs. In the PACOSS experiment, the processor ran the LQG/LTR control law (36 states, 23 inputs and 10 outputs) at a 400-Hz sample rate.

Due to their 1.5-Hz natural frequency, the RMAs cannot control the low frequency rigid body dynamics of the DTA. Therefore, a relative LOS was defined to exclude rigid body modes from the control system. Thus, the controller acts strictly as a vibration suppression system. Figure 3 identifies four disturbance input points on the DTA. These disturbances could be from maneuvering thrusters or onboard equipment. The relative LOS response to these disturbance inputs was taken as the performance metric to be minimized by the controller

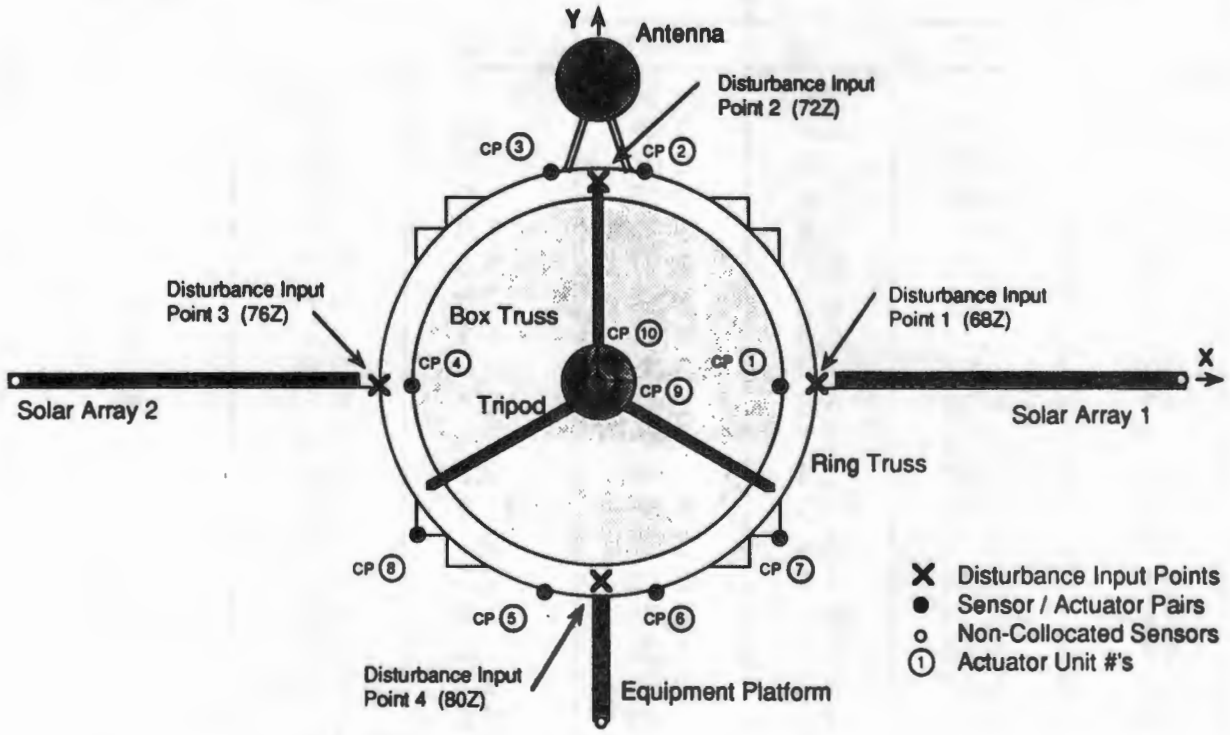

Figure 3. DTA Control Locations

In addition to the active control instrumentation, 182 Kistler model 8632 accelerometers were installed on the DTA for acquiring modal survey data. The large number of cables seen in Figure 2 are primarily from these modal accelerometers.

Tests with and without the majority of cables attached showed that the instrumentation cables had no effect on the flexible modes of the DTA. The LOS measurement was synthesized as a linear combination of selected measurements from the Kistler accelerometers.

A detailed finite element model of the DTA with over 10,000 degrees of freedom (DOF) was developed and test verified during the first phase of the PACOSS program. The detailed model was reduced (via a Guyan reduction) to 357 DOFs, and the modes determined from this reduced model. Table 1 compares the analytic and measured natural frequencies and damping ratios and lists the diagonal term of the orthogonality product between the predicted and identified modes up to 10 Hz. The modes retained in the control design model (CDM) were those possessing significant observability or controllability when the control points, sensor points, disturbance input points, and LOS were considered. Essentially, the CDM includes all global modes and a few appendage modes with frequencies below 10 Hz.

Table 1 Identified and Predicted Modes from DTA Modal Survey 3

Mode #	Measured		Analytic		X-orth diag.	Retained in control design model
	f_n (Hz)	ζ (%)	f_n (Hz)	ζ (%)		
1	1.03	2.9	1.04	4.8	0.97	
2	1.11	3.4	1.06	4.9	0.98	
3	2.59	3.9	2.68	2.8	0.98	X
4	3.03	7.4	3.17	5.9	0.51	
5	3.13	6.5	3.22	5.0	0.40	
6	3.30	5.1	3.37	5.3	0.71	X
7	3.45	8.7	3.54	7.4	0.74	X
8	3.73	6.3	3.75	4.9	0.98	X
9	4.12	7.4	3.85	10.1	0.98	
10	4.56	5.8	4.43	6.1	0.84	X
11	4.79	1.7	4.46	3.4	0.89	
12	4.82	1.6	4.46	3.0	0.89	
13	5.08	12.0	4.86	11.9	0.97	X
14	5.13	5.4	5.02	7.1	1.00	
15	5.78	1.6	5.85	2.6	0.94	X
16	5.82	2.1	5.85	2.5	0.98	X
17	6.49	5.0	6.00	3.3	0.96	
18	6.55	9.5	6.25	9.7	0.98	X
19	8.87	7.2	7.26	6.0	0.67	X
20	9.20	7.0	9.35	7.2	0.99	X
21	9.61	6.4	9.55	7.1	0.93	X
22	10.41	1.5	10.11	1.4	0.96	
23	10.49	1.4	10.11	1.4	0.94	

Note: Analytic damping ratios for modes 1 through 18 computed using VEM properties at 4 Hz, modes 19 through 23 computed using VEM properties at 9 Hz.

The correlation of the analytic and measured results was excellent in terms of frequency and damping ratios. The orthogonality diagonal term indicates agreement in terms of mode shape and should be greater than 0.9. As listed in Table 1, the mode shape correlation is quite good for most of the flexible modes retained in the CDM with the exception of modes 6, 7, 10, and 19. Modes 6 and 7 are antisymmetric global modes which involve the box truss, tripod, and solar arrays. Modes 10 and 19 are more local in nature, mainly involving the antenna.

Review of component modal surveys (Ref 6) indicated that the fundamental constrained interface mode of the box truss was about 6% higher in natural frequency than predicted. In an effort to evaluate the effect on the DTA system modes of matching the box truss constrained interface fundamental frequency, the 1/8-in. diameter x 0.014-in. wall box truss members were stiffened by 20%. This increased the box truss constrained interface fundamental frequency by the desired 6% to match the component test results. In this case, the fundamental mode shape of the box remained essentially unchanged. The DTA model was recoupled with the stiffened box model, and the system modes computed.

Table 2 lists the results for the updated model CDM modes. Note the negligible differences in natural frequencies and damping ratios between the two analytic models for all but modes 6 and 7 (see Table 1). These modes show a small shift in frequency but a relatively large change in damping ratio. Agreement with the measured values, while remaining quite good, improves somewhat for mode 7 but degrades slightly for mode 6. The orthogonality product diagonals for modes 6 and 7 between the measured and updated analytic modes are greatly improved as compared with the original DTA model. These results indicate that accurate prediction of closely spaced modes can be quite difficult. Here, a 6% change in a substructure modal frequency produced a major change in two very closely spaced system mode shapes. The task of predicting and identifying closely spaced modes in dynamically complex structures indeed requires extremely accurate finite element models.

Table 2 Measured and Analytic f_n and ζ for DTA Modes Retained in CDM

Mode #	Measured		Updated		X-orth diagonal
	f_n (Hz)	ζ (%)	f_n (Hz)	ζ (%)	
3	2.59	3.9	2.66	2.8	0.99
6	3.30	5.1	3.47	4.2	0.93
7	3.45	8.7	3.51	8.6	0.95
8	3.73	6.3	3.70	4.8	0.98
10	4.56	5.8	4.43	6.0	0.82
13	5.08	12.0	4.86	12.1	0.97
15	5.78	1.6	5.85	2.6	0.94
16	5.82	2.1	5.85	2.5	0.98
18	6.55	9.5	6.41	9.9	0.99
19	8.87	7.2	7.27	6.0	0.67
20	9.20	7.0	9.41	7.1	0.99
21	9.61	6.4	9.58	7.2	0.93

These observations indicate that DTA modes in the 3 to 4-Hz range are very sensitive to the relative stiffnesses of the box truss, tripod, and solar arrays. Stiffening the box truss seems to have improved correlation, but altering the tripod or solar array models may have similar effects. The DTA model with the stiffened box truss was used as the evaluation model for control performance evaluation. However, the original DTA model was used to design the LQG/LTR control since it was the best available model before conducting the final open loop modal survey in the 10 actuator DTA configuration.

LQG/LTR DESIGN APPROACH

Modern state-space control design techniques allow the analyst to conveniently model and analyze high-order, multi-input, multi-output (MIMO) systems. One branch of modern control theory well suited to the DTA vibration suppression problem is optimal LQG control. The LQG approach provides a framework in which LOS jitter suppression may be traded against active control effort to determine the most efficient compensator design for the required performance. The complete LQG/LTR design algorithm utilizes standard LQG design techniques (optimal regulator or estimator design, depending on the problem), and then computes the companion estimator or regulator design such that the singular values of the system loop-transfer matrix approach those of the full-state design case. This is known as "recovery" of loop-transfer functions (LTF).

The LQG control structure is shown in Figure 4. It consists of a Kalman-Bucy filter (KBF) with gains, $\mathbf{K_f}$, designed to estimate the states of a nominal plant model, $\mathbf{G(s)}$, and a full-state, linear-quadratic regulator, $\mathbf{K_c}$. Figure 4 and the nomenclature used here were taken from Reference 7. Referring to Figure 4, the following properties for the LQG control structure may be stated:

1) The LTF obtained by breaking the LQG loop at point **(I)'** is the KBF LTF $\mathbf{C\Phi K_f}$.

2) The LTF obtained by breaking the LQG loop at point **(I)** is **GK**. It can be made to approach $\mathbf{C\Phi K_f}$ pointwise in **s** by designing the LQR in accordance with a "sensitivity recovery" procedure due to Kwakernaak (Ref 8). This assumes $\mathbf{G(s)}$ is minimum phase and that $\mathbf{m \geq r}$.

3) The LTF obtained by breaking the LQG loop at point **(II)'** is the LQR LTF $\mathbf{K_c\Phi B}$.

4) The LTF obtained by breaking the LQG loop at point **(II)** is **KG**. It can be made to approach $\mathbf{K_c\Phi B}$ pointwise in **s** by designing the KBF in accordance with a "robustness recovery" procedure due to Doyle and Stein (Ref 9). This assumes $\mathbf{G(s)}$ is minimum phase and that $\mathbf{m \leq r}$.

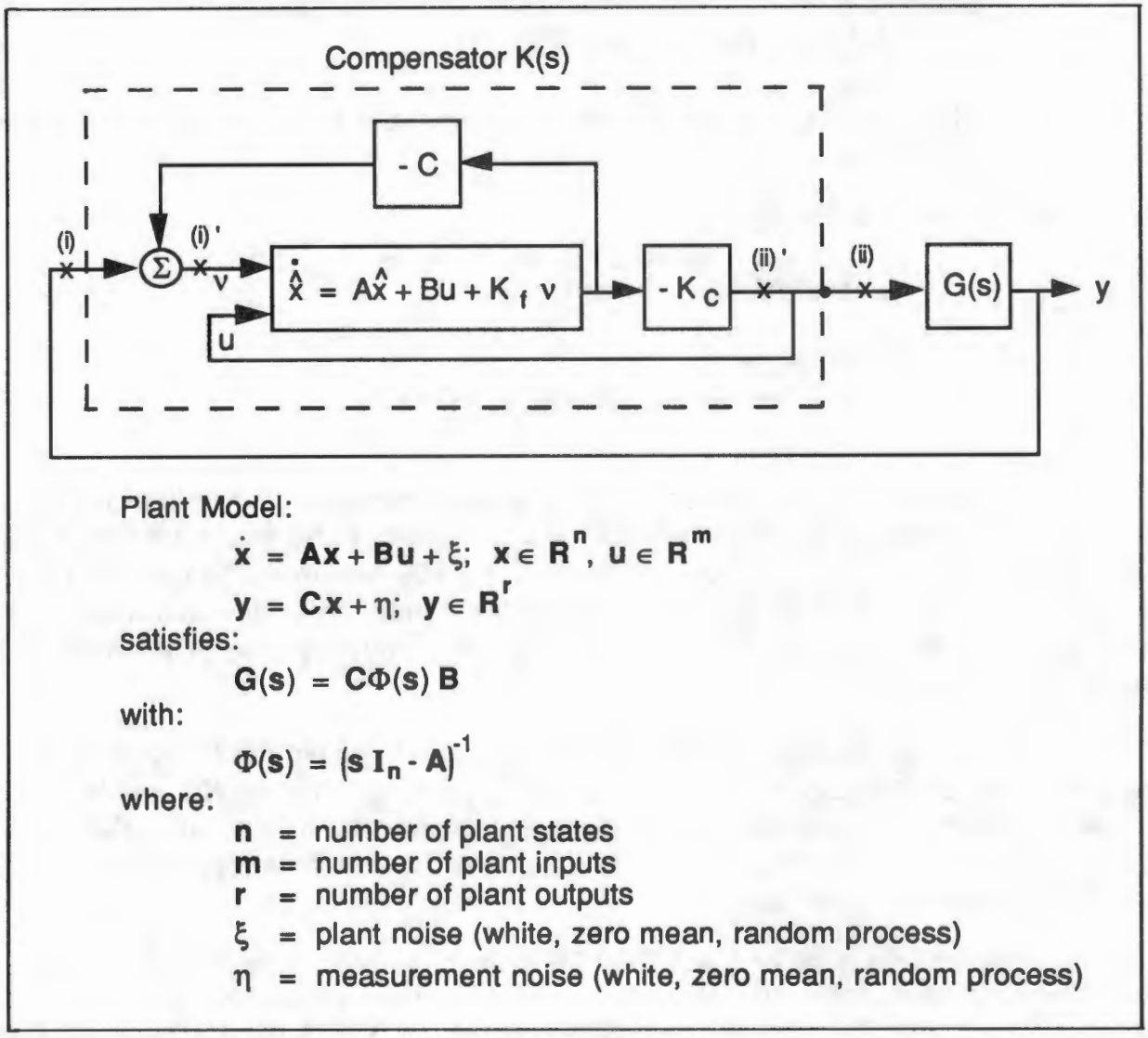

Plant Model:

$$\dot{x} = Ax + Bu + \xi; \quad x \in R^n, \; u \in R^m$$

$$y = Cx + \eta; \quad y \in R^r$$

satisfies:

$$G(s) = C\Phi(s)B$$

with:

$$\Phi(s) = (s I_n - A)^{-1}$$

where:

- **n** = number of plant states
- **m** = number of plant inputs
- **r** = number of plant outputs
- ξ = plant noise (white, zero mean, random process)
- η = measurement noise (white, zero mean, random process)

Figure 4. LQG Control Structure

As stated in Reference 7, "The significance of these four facts is that we can design LQG loop-transfer functions on a full-state feedback basis and then approximate them adequately with a recovery procedure."

The appropriate approach for the DTA is to design K_C via the LQR technique and then compute K_f to cause the singular values of the loop-transfer matrix, **KG**, to approach those of the full-state feedback case, $K_C\Phi B$. The procedure for computing the KBF gains is described in Reference 7 and summarized below:

1) Append dummy columns to **B** and zero rows to K_C to make $C\Phi B$ and $K_C\Phi B$ square (r x r). $C\Phi B$ must remain minimum phase.

2) Design the KBF with modified noise intensity matrices:

$$E(\xi\xi^T) = [M_o + q^2 B B^T]\delta(t-\tau)$$

$$E(\eta\eta^T) = N_o\delta(t-\tau)$$

where M_o, N_o are the nominal noise intensity matrices and **q** is a scalar parameter.

Under these conditions (Ref 9):

$$(1/q)K_f \rightarrow BWN_o^{-1/2} \text{ as } q \rightarrow \infty$$

where **W** is an orthonormal matrix.

This calculation of K_f results in:

$$K(s)\,G(s) \rightarrow K_C\Phi B \text{ as } q \rightarrow \infty$$

The design procedure for a MIMO system involves calculation of K_f with successively increasing values of the fictitious plant noise, **q**. As **q** approaches infinity, the singular values of **KG** will approach those of $K_C\Phi B$. However, the gains in K_f will become quite large, which is generally undesirable. Thus, a designer will wish to use the smallest **q** for which the LTF of **KG** acceptably matches that of $K_C\Phi B$ in the bandwidth of interest.

An extension of the single-input, single-output Bode plot for MIMO systems is the singular value (SV) Bode plot. Comparison of SV Bode plots for **KG** and $K_C\Phi B$ is a good indicator of the loop-transfer recovery achieved for a given value of **q**. Therefore, SV Bode plots may be used to determine the convergence of **KG** to $K_C\Phi B$ over the bandwidth of interest.

The design goal of the LQG/LTR control algorithm for the DTA was to minimize the LOS response to slew commands and noise disturbances at known input points. The approach taken for application to the DTA was to design an optimal regulator based on full-state feedback and then recover the loop-transfer functions at the disturbance and slew command input points. Thus, as discussed in Reference 10, the desirable characteristics of the LQR full-state feedback design are recovered by the estimator.

Calculation of the LQR gain matrix involves selection of state and control weighting matrices, **Q** and **R**. These required matrices were determined as follows:

$$\mathbf{LOS} = \begin{pmatrix} \mathbf{LOS\text{-}X} \\ \mathbf{LOS\text{-}Y} \end{pmatrix} = \begin{bmatrix} \mathbf{philosx} & 0 \\ \mathbf{philosy} & 0 \end{bmatrix} \begin{Bmatrix} \eta \\ \dot{\eta} \end{Bmatrix} = [\mathbf{TLOS}]\,\mathbf{x}$$

where:

philosx = mode shape coefficients defining LOS about X-axis
philosy = mode shape coefficients defining LOS about Y-axis
η = generalized modal coordinates

Minimize:

$$LOS^T[\bar{Q}]LOS + u^T[Ru] = x^T[TLOS^T][\bar{Q}][TLOS]x + u^T[R]u$$

Let:

$$R = I \ (10 \times 10)$$
$$Q = [TLOS^T][TLOS]\bar{Q}$$

The magnitude of the scalar $\bar{Q}$ is then varied to achieve the desired performance. Once the desired LOS response is achieved, representative disturbances and maneuvers are input to the full-state feedback closed-loop simulation to check if actuator stroke or force constraints are exceeded. If such limits are violated, the magnitude of **Q** must be reduced, and K_C recomputed.

After an acceptable LQR design is obtained, the KBF gain matrix is computed using the LTR method previously described. The input matrix, **B**, used in the loop-transfer recovery procedure includes the control and disturbance input points. Note that the number of points used (number of columns in **B**) must be less than or equal to the number of sensor measurements (number of rows in **C**). After each computation with a given value of **q**, the SV Bode plots of **KG** and $K_C\Phi B$ are compared. Once convergence (in a qualitative sense) is apparent, the control design is complete.

Following several iterations, good performance was achieved with a state-weighting parameter, **Q**, of 10^9. The LTR procedure was then performed for varying **q**. This process was conducted using the matrix algebra software package, PRO-MATLAB, and the Robust Control Toolbox function "ltru" (Ref 11). Figure 5 shows the convergence of the SV Bode plot for three values of **q**. The plots show nearly perfect agreement for $q = 10^6$. Using this value, the largest gain in the KBF matrix was 9600, which is large but proved to be acceptable.

The closed-loop frequencies and damping ratios for the initial LQG/LTR design coupled to the DTA CDM are listed in Table 3. Note that the LTR procedure resulted in several overdamped (real) poles far in the left half plane as well as several very low frequency real poles.

It was necessary to remove the high-frequency poles from the design to avoid aliasing problems when running the controller at 400 to 500 Hz. Also, since the 0.05-Hz bi-quad integrator poles were not included in the CDM, the low-frequency compensator poles could couple with the analog integrators used for the inertial velocity measurements and cause stability problems. Therefore, the compensator poles less than 0.5 Hz also had to be removed from the controller design.

In attempting to reduce the controller order, it was found that the low-frequency poles could not be removed from the compensator without causing instabilities when coupled with the DTA structural model. Therefore, the LQG/LTR design was repeated, but with a spectral shift applied to the Kalman filter design such

that the filter poles were required to be greater than 0.5 Hz. This procedure resulted in a compensator which indeed possessed no poles below 0.5 Hz, yet had performance nearly equivalent to the original design.

A reduced-order compensator was then obtained from the full-order design by removing compensator modes which had relatively small observability and controllability as determined from a balanced realization of the compensator formed using the PRO-MATLAB Robust Control Toolbox function, "obalreal" (Ref 11). This reduction removed most of the high-frequency compensator poles and several other relatively unimportant poles. A few remaining poles in the 100 to 400-Hz range were removed via a modal truncation, and the final compensator order was cut to 30 states, with a maximum frequency near 11 Hz. Figure 6 shows the SV Bode plot for full-state feedback, full-order compensator, and reduced-order compensator designs. Note that the maximum singular values agree nearly identically across the three cases.

In addition to the 30-state LQG/LTR compensator, three second-order bi-quad integrators were appended to the controller to derive inertial velocity from the non-collocated QA-1400 accelerometer measurements. Thus, the controller implemented in the Optima/3 involved 36 states with 23 inputs and 10 outputs. The Optima/3 was able to run the problem at a sample rate of 400 Hz.

Table 3. Initial DTA LQG/LTR Design Results

Complex Poles						Real Poles (rad/s)	
f_n (Hz)	ζ (%)	Type	f_n (Hz)	ζ (%)	Type		
0.12	10.00	S	3.43	7.12	E	-1.92×10^{-4}	-2.27×10^{3}
0.16	10.00	S	3.54	7.38	F	-1.97×10^{-4}	-2.67×10^{3}
0.17	10.00	S	3.78	6.25	F	-2.00×10^{-4}	-3.17×10^{3}
0.26	1.00	S	3.90	15.40	E	-3.22×10^{-4}	-3.51×10^{3}
0.26	1.00	S	4.44	6.05	E	-3.84×10^{-4}	-8.85×10^{4}
0.29	1.00	S	4.45	6.46	F	-9.99×10^{-4}	-8.86×10^{4}
0.29	1.33	E	4.71	16.99	F	-9.99×10^{-4}	-8.88×10^{4}
0.29	1.07	E	4.82	32.12	E	-9.99×10^{-4}	-8.97×10^{4}
0.29	1.00	E	5.25	29.92	F	-9.99×10^{-4}	-8.97×10^{4}
0.56	83.90	A	5.84	2.52	F	-9.99×10^{-4}	-9.12×10^{4}
0.73	26.66	A	5.85	2.55	F	-1.00×10^{-3}	-9.43×10^{4}
1.00	37.09	A	5.85	2.70	E	-1.00×10^{-3}	-9.46×10^{4}
1.38	61.22	A	5.86	2.88	E	-1.00×10^{-3}	-9.53×10^{4}
1.50	5.03	A	6.73	45.26	E	-7.96×10^{-2}	-9.63×10^{4}
1.50	5.03	A	7.34	6.42	F		
1.50	5.03	A	7.39	6.23	E		
1.51	5.09	A	8.94	13.87	F	NOTE:	
1.51	5.03	A	8.98	7.79	E	S = Suspension Mode	
1.53	5.02	A	10.06	22.51	F	A = Actuator Mode	
2.78	18.60	F	10.43	56.10	F	F = DTA Flexible Mode	
3.21	6.99	E	10.61	44.63	E	E = Estimator Mode	

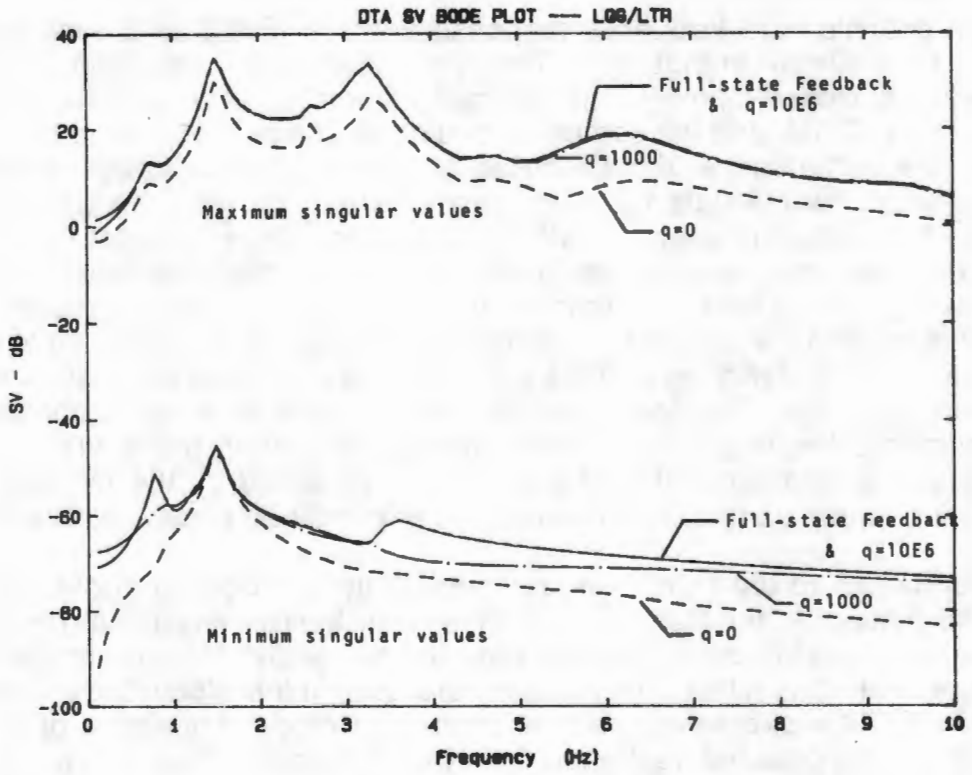

Figure 5. DTA SV Bode Plot, LQG/LTR

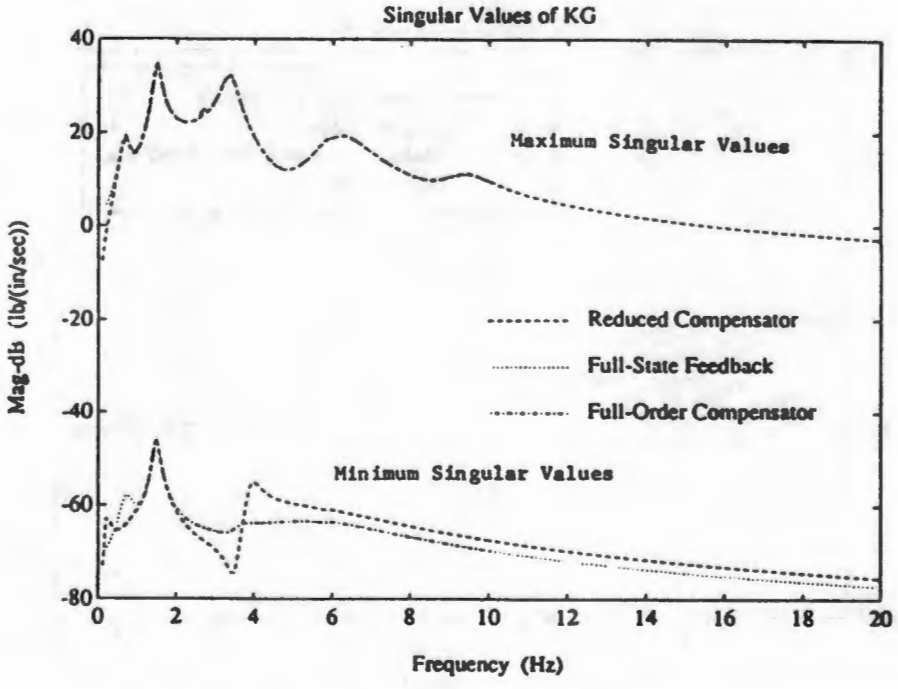

Figure 6. SV Bode Plot Comparing Full-State Feedback, Full-Order Compensator, and Reduced-Order Compensator for LQG/LTR Control

The analytic LOS frequency response function (FRF) for a slew command about the Y-axis is shown in Figure 7. The four traces show open-loop, closed-loop full-state feedback, closed-loop with the reduced-order state estimator designed using LTR coupled to the CDM, and the same reduced order compensator coupled to the full DTA model. The performance of the reduced-order compensator design on the CDM is very near that of the full-state feedback case, thereby showing the success of the LTR and reduction design process. The FRFs shown in Figure 7 indicate a 70 to 80% reduction in the root mean square (RMS) LOS jitter level based on response to white noise between 2 and 10 Hz. Another demonstration of the predicted control effectiveness is seen in the simulated slew response shown in Figure 8. Note that due to the passive damping designed into the DTA, only a few modes are significant in the open loop slew response. The active control system serves as a high authority control to virtually eliminate the response of these modes. Together, these FRFs and time response show the dramatic vibration suppression achieved by the modern optimal regulator design approach, and the effectiveness of combined passive/active control.

A drawback to the LQR method is sensitivity to modeling errors. While the design can be evaluated for stability robustness and bandwidth, actual performance can be seriously degraded by differences between the analytic design model and the actual structure. Recall that two DTA models were used in this study: the pretest model from which the CDM was created, and the evaluation model, consisting of all modes below 20 Hz of the updated (stiffened box truss) model. The following section discusses analytic results for both these models and presents corresponding measured data.

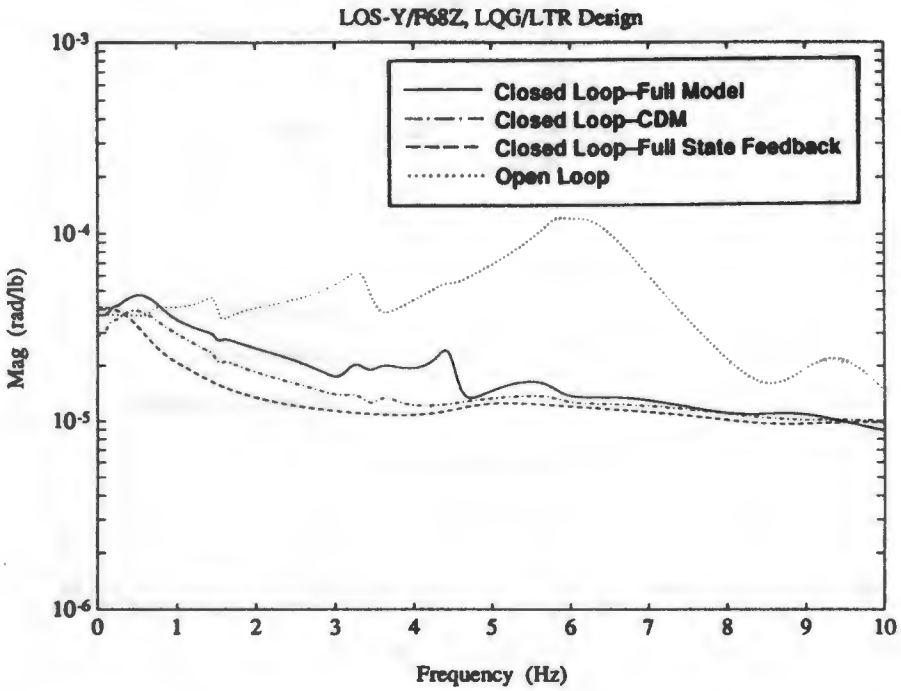

Figure 7. Analytic DTA LOS About Y-Axis

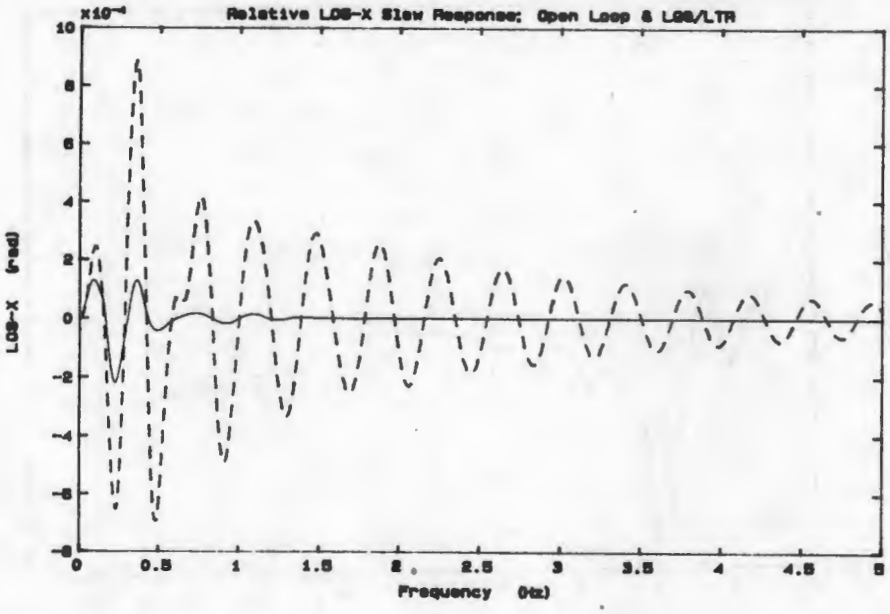

Figure 8. Relative LOS Slew Response, X-Axis

RESULTS

Open and closed loop FRFs were measured using burst random excitation at disturbance input points 68Z and 72Z (see Figure 3). Measurements were made for all the points which participate in the LOS, and the experimental LOS FRFs were computed as a linear combination of the actual measurements. Figure 9 shows the experimental open and closed loop FRFs for the LOS about the Y-axis due to excitation at point 68Z. The somewhat noisy closed loop response is a result of very low amplitude measurements being scaled by relatively large terms in the LOS computation. The corresponding analytic predictions, based on the original DTA model including all modes to 20 Hz, are shown in Figure 10. Note that while there is good qualitative agreement between the actual measurement and prediction for the open loop DTA, the LQG/LTR closed loop LOS measurement deviates significantly from predicted between 3 and 5 Hz. The cause of this error was, in part, due to the box truss component model. When the compensator was coupled to the updated DTA model, the FRF shown in Figure 11 resulted. This FRF shows a behavior very similar to that observed in the 3 to 5-Hz range. However, the overall response suppression is still less than predicted A rough calculation of the actual RMS jitter reduction achieved by the control gives 63% versus 74% predicted using the updated DTA model.

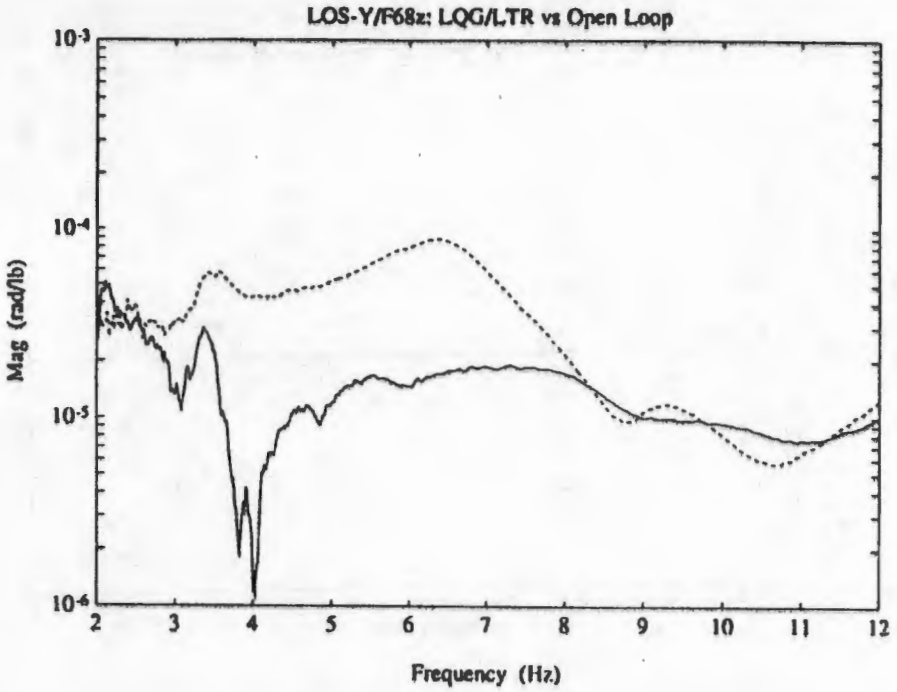

Figure 9 Experimental LOS FRF; LOS-Y/F68Z

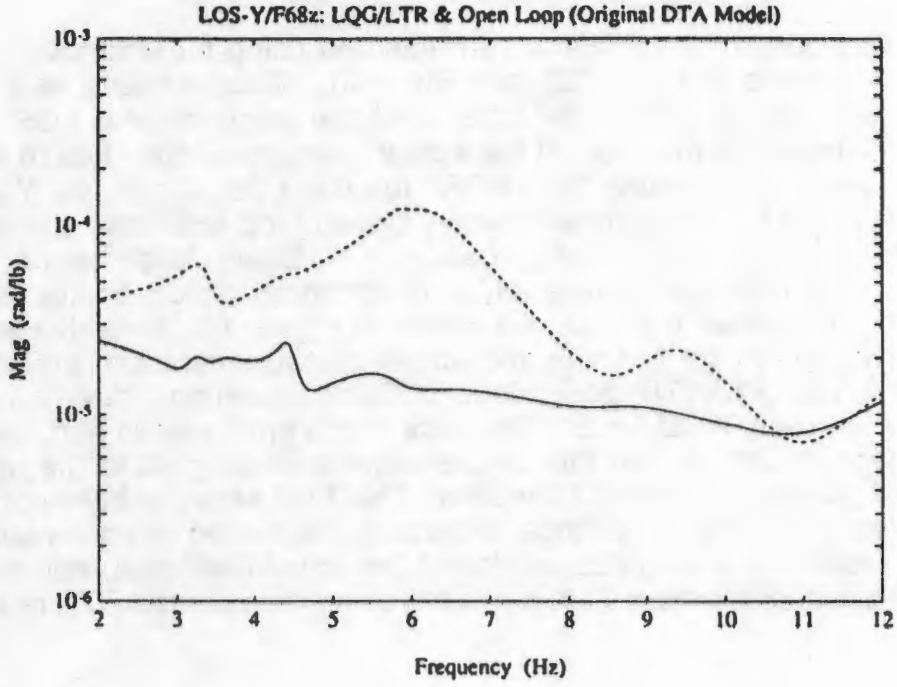

Figure 10 Predicted LOS-Y/F68Z; Original DTA Model

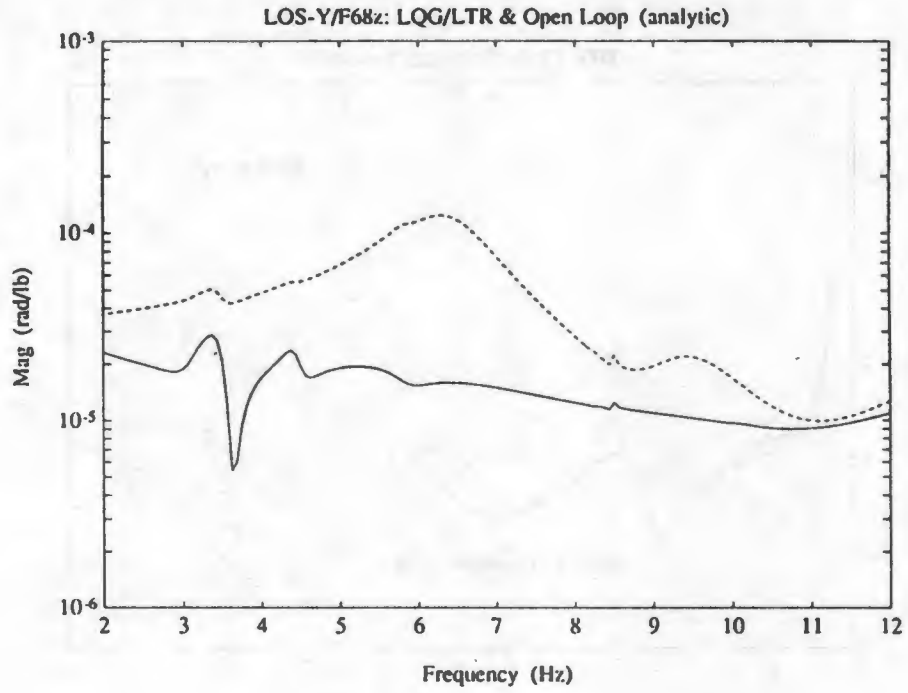

Figure 11 Predicted LOS-Y/F68Z; Updated DTA Model

The FRFs at selected control points demonstrated additional problems with the LQG/LTR design. Figure 12 shows the FRF between 72Z and CP2, and Figures 13 and 14 show the corresponding analytic FRFs using the original and updated DTA models respectively. Note the amplification of the closed loop FRF near 6 Hz. Apparently, a DTA mode near 6 Hz is being destabilized even though the open loop modal survey results indicated that the DTA flexible modes in this frequency range were accurate. As shown by the analytic FRFs, this is not predicted by either DTA model. Also, the control effectiveness at 3 Hz is much less than predicted. These observations indicate that the LQG/LTR design is quite sensitive to small differences between the CDM and actual structure.

Finally, Figure 15 shows a measured free decay for open and closed loop operation. This trace was produced by purely exciting the 2.6-Hz mode; perhaps the most accurately predicted mode of the DTA. The LQG/LTR control law did successfully apply a great amount of damping (on the order of 20% modal viscous) to this mode.

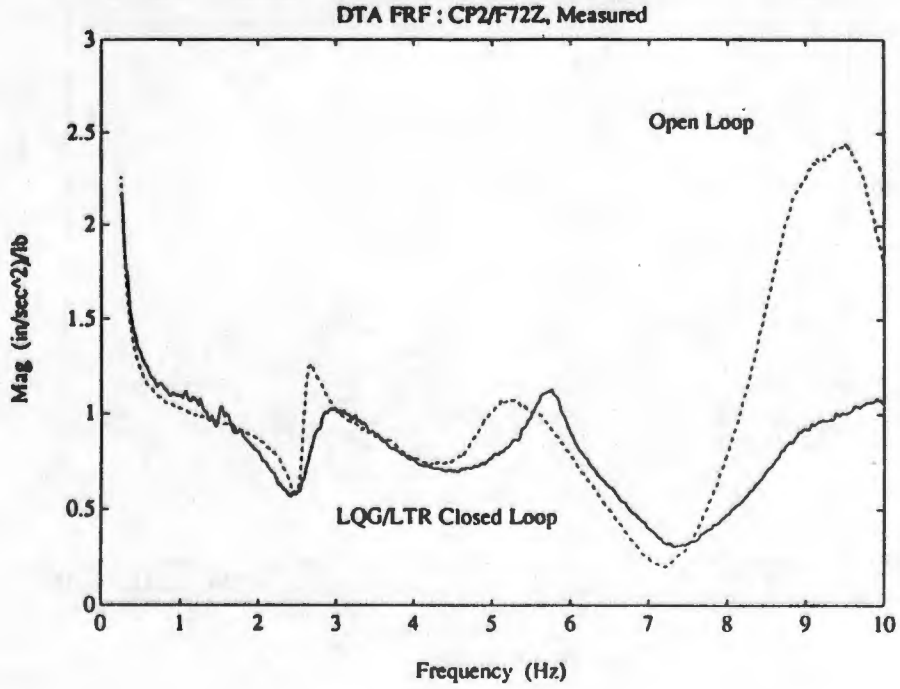

Figure 12 Measured DTA FRF; CP2/F72Z

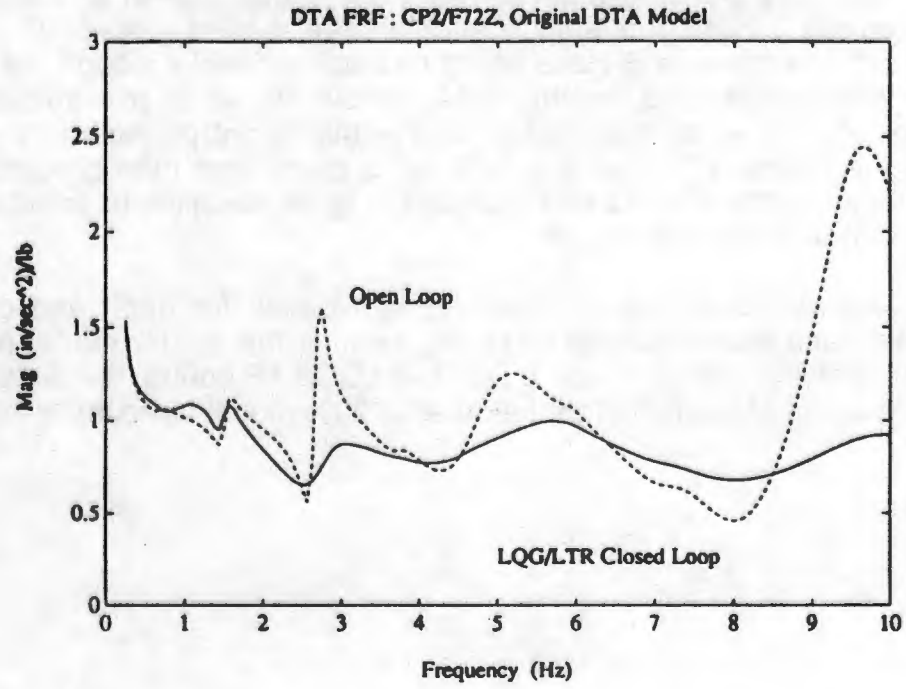

Figure 13 Predicted DTA FRF; CP2/F72Z, Original DTA Model

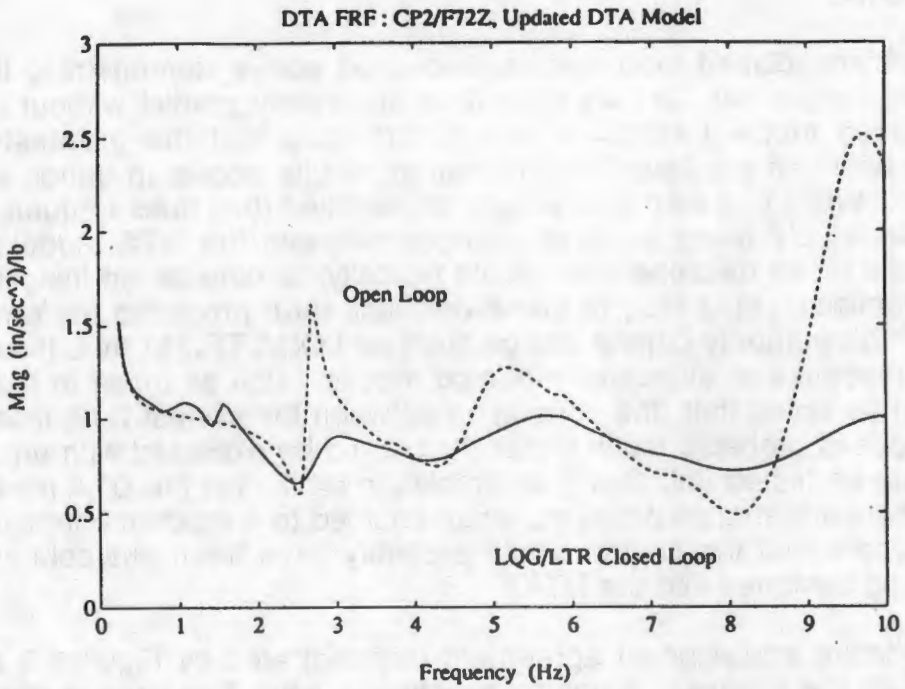

Figure 14 Predicted DTA FRF; CP2/F72Z, Updated DTA Model

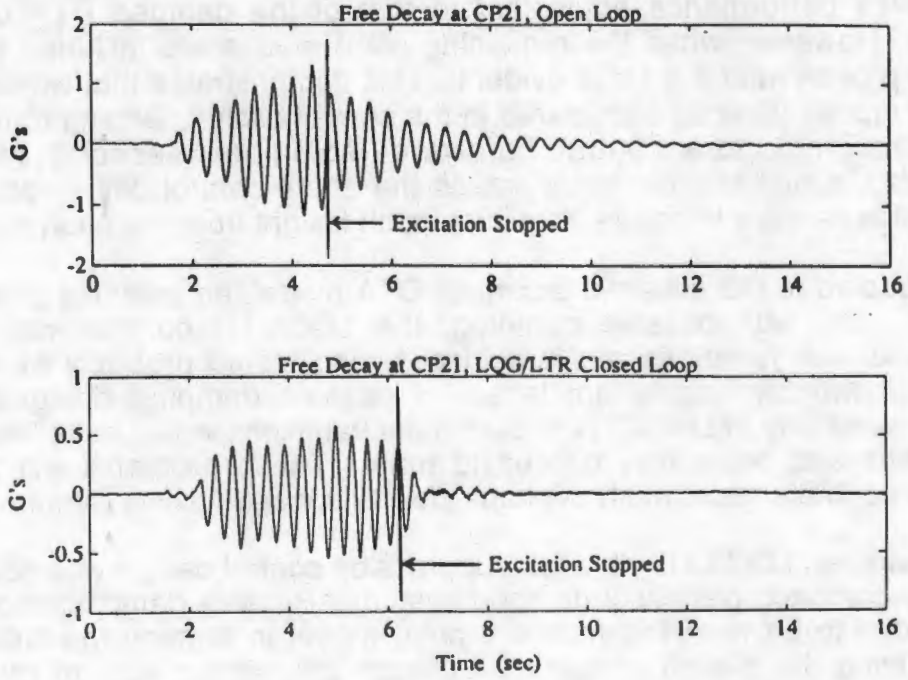

Figure 15 Free Decay of 2.6-Hz Mode

CONCLUSIONS

The open and closed loop results discussed above demonstrate that closely spaced flexible modes can be very difficult to accurately predict without resorting to empirically based model tuning. It is not surprising that the greatest degree of disagreement between predicted and measured results occurs in bands with closely spaced modes. While one source of error was identified (box truss frequency 6% low), there are undoubtedly many small differences between the DTA model and actual structure. While these discrepancies would typically be considered insignificant by a structural dynamicist, they lead to somewhat less than predicted performance of a sophisticated high authority control design such as LQG/LTR. In fact, the control law amplified the response of even well modeled modes, such as those in the 5 to 7-Hz range. It must be noted that the correlation between the pretest DTA model and the measured modes is probably much better than could be expected with an actual LSS which would not be tested until being assembled in orbit. Yet the DTA model still fails to predict critical performance problems when coupled to a modern controller. In fact, the results indicate that the control would probably have been unstable without the passive damping designed into the DTA.

The qualitative analysis/test agreement demonstrated by Figures 9 through 11 serves to validate the analysis. A natural question is; what if no passive damping were designed into the DTA? To answer this, an LQG/LTR design was performed for the original DTA model with only 0.2% modal viscous damping in all modes. As demonstrated by the DTA ring truss component modal survey (Ref 5), and the PACOSS D-Strut truss discussed in Reference 12, this level of damping would be expected from a tight, precision structure with no intentional damping designed in. The results of this design are shown in Figure 16. Note that the full-state feedback design achieves performance equivalent to that of the damped DTA closed loop performance. However, when the remaining plant modes are included in the plant model, a sharp peak near 4.5 Hz is evident. This demonstrates that without passive control, more modes must be considered in the control design, leading to higher order controllers requiring more control hardware (actuators, sensors) with greater capability. Also, a higher order plant makes the entire control design process more difficult since it is iterative in nature, requiring much insight from the analyst .

When coupled to the stiffened box truss DTA model, an unstable pole at 3.5 Hz was present. So, with passive damping, the LQG/LTR control was marginally successful, and with iterations and empirical tuning, could probably be made very effective. But without significant levels of passive damping designed into the structure, the sensitivity of LQG/LTR to parameter variations would have lead to closed loop instabilities and been very difficult to tune. These problems will be present whenever the controller bandwidth overlaps closely spaced flexible modes.

In summary, an LQG/LTR vibration suppression control design was conducted for a dynamically complex, passively damped system. Passive damping allowed many structural modes to be removed from the plant model in forming the CDM, thereby greatly simplifying the design process. Although only about 80% of the predicted closed loop performance was achieved, the design was stable and did significantly suppress LOS vibrations. Some structural modes were amplified, but the relatively

high passive damping designed into the structure maintained stability. The results of this experiment demonstrate that if high bandwidth, high authority modern control algorithms are to be successfully applied to LSS, passive damping must be designed into the LSS from the start.

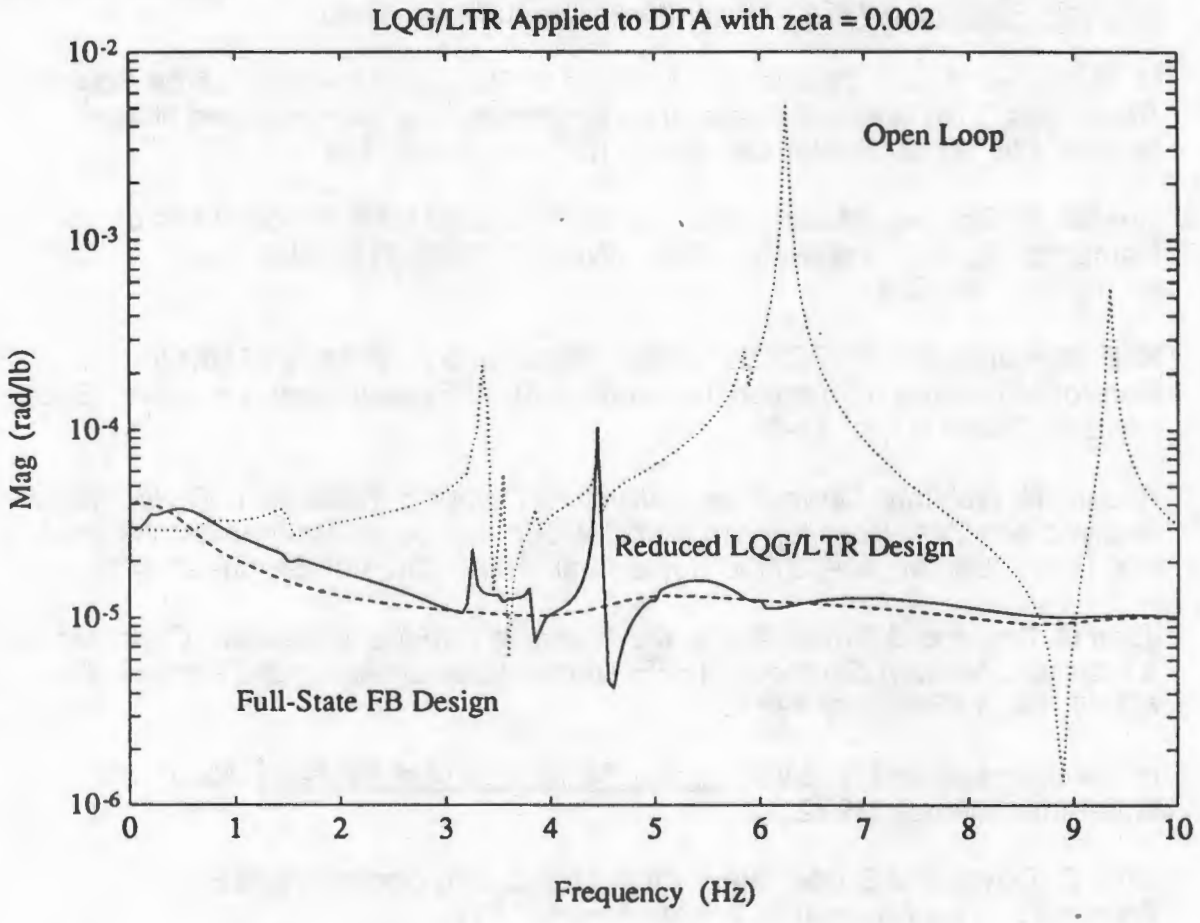

Figure 16 LQG/LTR Design with Nominally Damped DTA (zeta = 0.002)

ACKNOWLEDGEMENT

This work was supported by the Air Force Flight Dynamics Laboratory Wright Research and Development Center under the Passive and Active Control of Space Structures (PACOSS) Program, Contract Number F33615-82-C-3222.

REFERENCES

1. Russell N. Gehling, *PACOSS Dynamic Test Article*, Proceedings of Damping '91, San Diego, CA, 13-15 February 1991.

2. PACOSS Final Report, Volume 2, Dynamic Test Article Modal Survey: Test and Analysis Results, (WRDC-TR-90-3044), September, 1990.

3. D. R. Morgenthaler, *Design and Analysis of Passively Damped Large Space Structures,* 11th Biennial Conference on Mechanical Vibration and Noise, Boston, MA, 27-30 September, 1987, (DE-Vol. 5), pp. 1-8.

4. Russell N. Gehling, *Modal Survey of the PACOSS DTA*, Proceedings of Damping '89, 8-10 February, 1989, (WRDC-TR-89-3116, Vol. III), pp. KCC-1 - KCC-31.

5. K. E. Richards, Jr., *PACOSS Program Status and Results*, NASA/DOD Control/Structures Interaction Technology 1989 Proceedings, February 1989, (NASA CP-3041), pp. 31-65.

6. Russell N. Gehling, *Large Space Structure Damping Treatment Performance: Analytic and Test Results,* 11th Biennial Conference on Mechanical Vibration and Noise, Boston, MA, 27-30 September, 1987, (DE-Vol. 5), pp. 93-100.

7. John C. Doyle and Gunter Stein, *Multivariable Feedback Design: Concepts for a Classical/Modern Synthesis*, IEEE Transactions on Automatic Control, Vol. AC-26, No. 1, February 1981.

8. H. Kwakernaak and R. Sivan, Linear Optimal Control Systems, New York, Wiley-Interscience, 1972.

9. John C. Doyle and Gunter Stein, *Robustness with Observers,* IEEE Transactions on Automatic Control, August 1979.

10. D. Brett Ridgely and Siva S. Banda, Introduction to Robust Multivariable Control, AFWAL-TR-85-3102, February, 1986.

11. Richard Y. Chiang and Michael Safonov, Robust Control Toolbox Users Guide, The MathWorks, Inc., South Natick, MA, June 1988.

12. D. R. Morgenthaler, *Design, Analysis, and Testing of the PACOSS D-Strut Truss*, Proceedings of Damping '91, San Diego, CA, 13-15 February 1991.